ACP
Articles | Volume 21, issue 10
https://doi.org/10.5194/acp-21-7651-2021

Modulation of radiative aerosols effects by atmospheric circulation over the Euro-Mediterranean region

Anna Luise Merk1, Johannes Quaas1, Susanne Crewell2, Marc Mallet3, Martina Michaela4, Dominique Bouniol5, Bertrand Decharme6, Thomas Drugé3, Roland Seiz7, and Stefan Bühler2 ... Show more author details

1Leipzig Institute for Meteorology, University of Leipzig, Germany, 2Meteorologisches Institut, Universität Hamburg, Germany, 3CNRS, CNRM/GAME, Toulouse, France, 4Max Planck Institute for Meteorology, Hamburg, Germany, 5CNRS, CNRM/CEN, Toulouse, France, 6CNRS, CNRM/CNRM, Toulouse, France, 7Independent consultant, Switzerland

Received: 20 Dec 2019 – Discussion started: 27 Jan 2020 – Revised: 19 May 2020 – Accepted: 24 Nov 2020 – Published: 17 Jul 2021

Abstract

Click here to hide Abstract

Climate models serve all better understanding regional climate aerosol interactions. In this study, we investigate the modulation of aerosol radiative effects by atmospheric circulation over the Euro-Mediterranean region. The aerosol optical properties (AOP) 2020 have been carried out using the Tropospheric Ultraviolet and Visible (TUV) radiation model and combined with climatologies of aerosol optical properties and meteorological reanalysis data. We use the Tracking and Diagnosing Cyclones Potential Intensity Climatology (TDCPIC) to quantify aerosol properties in cyclones, anticyclones, and their surroundings. We find that the aerosol optical properties are influenced by the atmospheric circulation in terms of different climate and aerosol parameters. The evaluation shows a good agreement between the simulated aerosol optical properties and climatological data. We find that cyclones reduce aerosol optical depth (AOD) and aerosol radiative effects (ARE) in their surroundings. The aerosol interactions over this region. A first attempt to explain the climate variability of aerosol radiative effects (ARE) in the Euro-Mediterranean region, we find that the aerosol optical properties (AOP) are influenced by the atmospheric circulation. We find that aerosols over the Atlantic Ocean and the western Mediterranean, and in summer in the eastern Mediterranean, are influenced by anticyclones, which leads to an increase in AOD and ARE in their surroundings. In contrast, cyclones reduce AOD and ARE in their surroundings. In winter, in dry scale. The use of "weather regimes", namely persistency meteorological patterns, allows to explain the variability of aerosol radiative effects (ARE) in the Euro-Mediterranean region. We find that the aerosol optical properties (AOP) are influenced by the atmospheric circulation

and Crosnier, 2007) and already used in several studies (e.g. Karlsson et al., 2016; Kneen et al., 2020; Pfeifroth et al., 2018; Stengel et al., 2016; Trigo et al., 2011; Urraca et al., 2018; Urraca et al., 2020; Wild et al., 2013) for future CMSAF scientific datasets (CLARA-A3 and CLARA-A2.1 for future Copernicus Climate Change Service (C3S) datasets and for Fundamental Climate Data Record for Europe) for benchmarking and parameterization. The evaluation of the new version (v2.1) of the CLARA-A2 AOD against ground-based AOD from AERONET and other satellite AOD datasets has been thoroughly discussed in Karlsson et al. (2021). Based on it, CLARA-A2 AOD is the most accurate satellite AOD dataset calculated with an AUVOR-A retrieval (10%–15% correct) and with the version 2 of the SAFNWC/PPS AOD (10%–15% correct) among the satellite datasets assessed against AERONET AOD. Further, the spatial and temporal variability of AOD in Europe has been also thoroughly discussed in Karlsson et al. (2021).

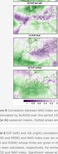

Figure 2 Entire (DJF, left) and summer (JJA, right) average differences between AUVOR-A and AVHRR/NOAA-18 (first row), SEVIRI/MSG-2 (second row), MODIS/Terra (third row) and MODIS/Aqua (fourth row) AOD. Data are shown in black lines, the land domain is shown in green, the sea domain in blue, the coastline in black, the lake in cyan, the ice in light blue, the snow in light red, the cloud in grey, the missing in white, and the outside area in white.

↑Download Free Version ↑ ↑Download AOD

Table 1 Average biases in the AUVOR-A retrievals (AUVOR) in terms of near-surface temperature (in °C) against those of the AVHRR/NOAA-18 (AVHRR), SEVIRI/MSG-2 (SEVIRI), Terra/MODIS (Terra) and Aqua/MODIS (Aqua) AOD and CLARA-A2 (CLARA) for the entire Europe (EUROPE), Mediterranean Sea (MEDITERRANEAN), Atlantic Ocean (ATLANTIC), and Scandinavian and Baltic Seas (SCANDINAVIA) for the entire year (ALL), winter (DJF) and summer (JJA) seasons. The number of pixels used for the comparison is also shown in the last column (N). Note that the AUVOR-A retrieval is not performed over the Mediterranean Sea, Atlantic Ocean and Scandinavian and Baltic Seas.

	AUVOR	AVHRR	SEVIRI	Terra	Aqua	CLARA	N
EUROPE ALL	0.08	0.09	0.09	0.09	0.09	0.09	1.0E+07
EUROPE DJF	0.07	0.08	0.08	0.08	0.08	0.08	2.0E+06
EUROPE JJA	0.09	0.09	0.09	0.09	0.09	0.09	2.0E+06
MEDITERRANEAN ALL		0.09	0.09	0.09	0.09	0.09	1.0E+07
MEDITERRANEAN DJF		0.08	0.08	0.08	0.08	0.08	2.0E+06
MEDITERRANEAN JJA		0.09	0.09	0.09	0.09	0.09	2.0E+06
ATLANTIC ALL		0.09	0.09	0.09	0.09	0.09	1.0E+07
ATLANTIC DJF		0.08	0.08	0.08	0.08	0.08	2.0E+06
ATLANTIC JJA		0.09	0.09	0.09	0.09	0.09	2.0E+06
SCANDINAVIA ALL		0.09	0.09	0.09	0.09	0.09	1.0E+07
SCANDINAVIA DJF		0.08	0.08	0.08	0.08	0.08	2.0E+06
SCANDINAVIA JJA		0.09	0.09	0.09	0.09	0.09	2.0E+06

↑Download Free Version ↑ ↑Download AOD

Table 2 Average biases in radiation (W·m^{-2}) in AUVOR-A/SEVIRI (AUVOR) relative to those of the AVHRR/NOAA-18 (AVHRR), SEVIRI/MSG-2 (SEVIRI) and Terra/MODIS (Terra) and Aqua/MODIS (Aqua) AOD and CLARA-A2 (CLARA) for the entire Europe (EUROPE), Mediterranean Sea (MEDITERRANEAN), Atlantic Ocean (ATLANTIC), and Scandinavian and Baltic Seas (SCANDINAVIA) for the entire year (ALL), winter (DJF) and summer (JJA) seasons. The number of pixels used for the comparison is also shown in the last column (N). Note that the AUVOR-A retrieval is not performed over the Mediterranean Sea, Atlantic Ocean and Scandinavian and Baltic Seas.

	AUVOR	AVHRR	SEVIRI	Terra	Aqua	CLARA	N
EUROPE ALL	0.0	0.0	0.0	0.0	0.0	0.0	1.0E+07
EUROPE DJF	0.0	0.0	0.0	0.0	0.0	0.0	2.0E+06
EUROPE JJA	0.0	0.0	0.0	0.0	0.0	0.0	2.0E+06
MEDITERRANEAN ALL		0.0	0.0	0.0	0.0	0.0	1.0E+07
MEDITERRANEAN DJF		0.0	0.0	0.0	0.0	0.0	2.0E+06
MEDITERRANEAN JJA		0.0	0.0	0.0	0.0	0.0	2.0E+06
ATLANTIC ALL		0.0	0.0	0.0	0.0	0.0	1.0E+07
ATLANTIC DJF		0.0	0.0	0.0	0.0	0.0	2.0E+06
ATLANTIC JJA		0.0	0.0	0.0	0.0	0.0	2.0E+06
SCANDINAVIA ALL		0.0	0.0	0.0	0.0	0.0	1.0E+07
SCANDINAVIA DJF		0.0	0.0	0.0	0.0	0.0	2.0E+06
SCANDINAVIA JJA		0.0	0.0	0.0	0.0	0.0	2.0E+06

↑Download Free Version ↑ ↑Download AOD

Figure 3 presents the biases of the AUVOR-A retrieval against those of the AVHRR, SEVIRI and MODIS AOD for the entire year (left) and for the summer (right) for the entire Europe. Similar biases are expected for the CLARA AOD. Table 1 shows the average biases in the AUVOR-A retrieval against those of the AVHRR, SEVIRI, Terra and Aqua AOD and CLARA AOD for the entire year (ALL), winter (DJF) and summer (JJA) seasons in Europe (on average, +/-0.4 and +/-0.5 W·m^{-2} on average for the shortwave and longwave radiation, respectively, for the entire year). Table 2 shows the same but for the AUVOR-A/SEVIRI radiation against those of the AVHRR/NOAA-18, SEVIRI/MSG-2, Terra/MODIS and Aqua/MODIS AOD and CLARA AOD. Table 2 also shows the number of pixels used for the comparison in each case. Note that the AUVOR-A retrieval is not performed over the Mediterranean Sea, Atlantic Ocean and Scandinavian and Baltic Seas. Table 2 also shows that the AUVOR-A/SEVIRI radiation is in the range of those of the other AVHRR/NOAA-18, SEVIRI/MSG-2, Terra/MODIS and Aqua/MODIS AOD and CLARA AOD for the entire Europe (on average, +/-0.1 W·m^{-2} for the shortwave and longwave radiation, respectively, for the entire year). Table 2 also shows that the AUVOR-A/SEVIRI radiation is in the range of those of the other AVHRR/NOAA-18, SEVIRI/MSG-2, Terra/MODIS and Aqua/MODIS AOD and CLARA AOD for the Mediterranean Sea, Atlantic Ocean and Scandinavian and Baltic Seas (on average, +/-0.1 W·m^{-2} for the shortwave and longwave radiation, respectively, for the entire year). Table 2 also shows that the AUVOR-A/SEVIRI radiation is in the range of those of the other AVHRR/NOAA-18, SEVIRI/MSG-2, Terra/MODIS and Aqua/MODIS AOD and CLARA AOD for the Mediterranean Sea, Atlantic Ocean and Scandinavian and Baltic Seas (on average, +/-0.1 W·m^{-2} for the shortwave and longwave radiation, respectively, for the entire year). Table 2 also shows that the AUVOR-A/SEVIRI radiation is in the range of those of the other AVHRR/NOAA-18, SEVIRI/MSG-2, Terra/MODIS and Aqua/MODIS AOD and CLARA AOD for the entire Europe (on average, +/-0.1 W·m^{-2} for the shortwave and longwave radiation, respectively, for the entire year). Table 2 also shows that the AUVOR-A/SEVIRI radiation is in the range of those of the other AVHRR/NOAA-18, SEVIRI/MSG-2, Terra/MODIS and Aqua/MODIS AOD and CLARA AOD for the Mediterranean Sea, Atlantic Ocean and Scandinavian and Baltic Seas

Figure 5a: Averaged LSTB (CRU) correlations with teleconnection indices for winter (DJF), spring (MAM), summer (JJA) and whole year (annual) mean surface temperatures (1x1°) with ERA-Interim data for the period 1979-2020. Only values above statistical 95% confidence level are shown. Indices used are the North Atlantic Oscillation (NAO), East Atlantic (EA), Scandinavian (SCAND), East Atlantic/Western Russia (EAWR) and East Atlantic/Mediterranean (EAMT) patterns, see Supplementary Figure 1 for their maps.

Figure 5b: Same as Figure 5a, but for the period 1950-2020.

Winter (DJF) is the most active season for the NAO and EA teleconnections, which explains a large part of the variability in surface temperatures (Figure 5a). The NAO is the strongest teleconnection in Europe, and its positive phase is associated with warm temperatures across the continent, especially in its northwestern parts, which explain a large part of the correlation between NAO and the LSTB (Figure 6a). The EA is the second most important teleconnection in winter, and its positive phase is also linked to the increase in the LSTB, but its spatial footprint is more in the southern parts of Europe, with the Mediterranean of relatively stable or moderately decreasing trend over Iberia, while the Scandinavian (SCAND) and the East Atlantic/Western Russia (EAWR) patterns have more regional impacts, for the positive phase of SCAND cooling in most of Europe except for the Iberian Peninsula and southern France, and for the positive phase of EAWR cooling in Eastern Europe.

With regards to surface seasonal (one month) means greenhouse gas emissions which are not dominated by the LSTB, the NAO is the most important in winter, but its spatial footprint is much smaller and is a higher resolution than the LSTB (Figure 6b). The EA is the second most important in the positive NAO conditions. However, this pattern is not robust in total NAO due to the opposite sign in its negative phase (Figure 6c).

Figure 5c: Same as Figure 5a, but for the period 1950-1979.

Figure 5d: Same as Figure 5a, but for the period 1980-2020.

Figure 5d (period 1980-2020) shows the strongest correlations between the LSTB and the teleconnections, which explains a large part of the correlation between NAO and the LSTB (Figure 6a). The increase over time in the importance of the NAO and EA in the LSTB is also evident from the comparison of Figure 5c and 5d. The increase over time in the importance of the NAO and EA in surface temperature is also evident in the GHG fluxes, which explain a large part of the correlation between NAO and the GHG fluxes (Figure 6b). The increase over time in the importance of the NAO and EA in surface temperature is also evident in the GHG fluxes, which explain a large part of the correlation between NAO and the GHG fluxes (Figure 6b). The increase over time in the importance of the NAO and EA in surface temperature is also evident in the GHG fluxes, which explain a large part of the correlation between NAO and the GHG fluxes (Figure 6b).

Figure 5e: Same as Figure 5a, but for the period 1950-1979.

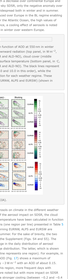

Figure 5f: Same as Figure 5a, but for the period 1980-2020.

Figure 5e (period 1950-1979) shows the strongest correlations between the LSTB and the teleconnections, which explains a large part of the correlation between NAO and the LSTB (Figure 6a). The increase over time in the importance of the NAO and EA in surface temperature is also evident in the GHG fluxes, which explain a large part of the correlation between NAO and the GHG fluxes (Figure 6b). The increase over time in the importance of the NAO and EA in surface temperature is also evident in the GHG fluxes, which explain a large part of the correlation between NAO and the GHG fluxes (Figure 6b). The increase over time in the importance of the NAO and EA in surface temperature is also evident in the GHG fluxes, which explain a large part of the correlation between NAO and the GHG fluxes (Figure 6b).

Figure 5g: Same as Figure 5a, but for the period 1950-1979.

Figure 5h: Same as Figure 5a, but for the period 1980-2020.

Figure 5g (period 1950-1979) shows the strongest correlations between the LSTB and the teleconnections, which explains a large part of the correlation between NAO and the LSTB (Figure 6a). The increase over time in the importance of the NAO and EA in surface temperature is also evident in the GHG fluxes, which explain a large part of the correlation between NAO and the GHG fluxes (Figure 6b). The increase over time in the importance of the NAO and EA in surface temperature is also evident in the GHG fluxes, which explain a large part of the correlation between NAO and the GHG fluxes (Figure 6b). The increase over time in the importance of the NAO and EA in surface temperature is also evident in the GHG fluxes, which explain a large part of the correlation between NAO and the GHG fluxes (Figure 6b).

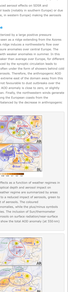

Figure 5i: Same as Figure 5a, but for the period 1950-1979.

Figure 5j: Same as Figure 5a, but for the period 1980-2020.

Figure 5i (period 1950-1979) shows the strongest correlations between the LSTB and the teleconnections, which explains a large part of the correlation between NAO and the LSTB (Figure 6a). The increase over time in the importance of the NAO and EA in surface temperature is also evident in the GHG fluxes, which explain a large part of the correlation between NAO and the GHG fluxes (Figure 6b). The increase over time in the importance of the NAO and EA in surface temperature is also evident in the GHG fluxes, which explain a large part of the correlation between NAO and the GHG fluxes (Figure 6b). The increase over time in the importance of the NAO and EA in surface temperature is also evident in the GHG fluxes, which explain a large part of the correlation between NAO and the GHG fluxes (Figure 6b).

Figure 5k: Same as Figure 5a, but for the period 1950-1979.

Figure 5l: Same as Figure 5a, but for the period 1980-2020.

Figure 5k (period 1950-1979) shows the strongest correlations between the LSTB and the teleconnections, which explains a large part of the correlation between NAO and the LSTB (Figure 6a). The increase over time in the importance of the NAO and EA in surface temperature is also evident in the GHG fluxes, which explain a large part of the correlation between NAO and the GHG fluxes (Figure 6b). The increase over time in the importance of the NAO and EA in surface temperature is also evident in the GHG fluxes, which explain a large part of the correlation between NAO and the GHG fluxes (Figure 6b). The increase over time in the importance of the NAO and EA in surface temperature is also evident in the GHG fluxes, which explain a large part of the correlation between NAO and the GHG fluxes (Figure 6b).

4.2 Jet Stream (JTA)

In summer, the interannual variability of NAO is less important than in winter, as indicated by the smaller correlations between the NAO and the LSTB (Figure 5a). The EA is the most important teleconnection in summer, and its positive phase is associated with a decrease in the LSTB in most of the Atlantic Ocean, southern Europe and the Mediterranean but not over Eastern Europe (Figure 5a). The EA is also the most important in the GHG fluxes in summer, and its positive phase is associated with a decrease in the GHG fluxes in most of Europe (Figure 5b). The SCAND is the second most important teleconnection in summer, and its positive phase is associated with positive GHG fluxes in most of Europe (Figure 5b). The increase in surface NAO could be due to an increase in the JTA (Figure 7a). The increase in surface NAO could be due to an increase in the JTA (Figure 7a). The increase in surface NAO could be due to an increase in the JTA (Figure 7a).

Figure 5a: Averaged LSTB (CRU) correlations with teleconnection indices for winter (DJF), spring (MAM), summer (JJA) and whole year (annual) mean surface temperatures (1x1°) with ERA-Interim data for the period 1979-2020. Only values above statistical 95% confidence level are shown. Indices used are the North Atlantic Oscillation (NAO), East Atlantic (EA), Scandinavian (SCAND), East Atlantic/Western Russia (EAWR) and East Atlantic/Mediterranean (EAMT) patterns, see Supplementary Figure 1 for their maps.

Figure 5b: Same as Figure 5a, but for the period 1950-2020.

Winter (DJF) is the most active season for the NAO and EA teleconnections, which explains a large part of the variability in surface temperatures (Figure 5a). The NAO is the strongest in Europe, and its positive phase is associated with warm temperatures across the continent, especially in its northwestern parts, which explain a large part of the correlation between NAO and the LSTB (Figure 6a). The EA is the second most important teleconnection in winter, and its positive phase is also linked to the increase in the LSTB, but its spatial footprint is more in the southern parts of Europe, with the Mediterranean of relatively stable or moderately decreasing trend over Iberia, while the Scandinavian (SCAND) and the East Atlantic/Western Russia (EAWR) patterns have more regional impacts, for the positive phase of SCAND cooling in most of Europe except for the Iberian Peninsula and southern France, and for the positive phase of EAWR cooling in Eastern Europe.

With regards to surface seasonal (one month) means greenhouse gas emissions which are not dominated by the LSTB, the NAO is the most important in winter, but its spatial footprint is much smaller and is a higher resolution than the LSTB (Figure 6b). The EA is the second most important in the positive NAO conditions. However, this pattern is not robust in total NAO due to the opposite sign in its negative phase (Figure 6c).

Figure 5c: Same as Figure 5a, but for the period 1950-1979.

Figure 5d: Same as Figure 5a, but for the period 1980-2020.

Figure 5d (period 1980-2020) shows the strongest correlations between the LSTB and the teleconnections, which explains a large part of the correlation between NAO and the LSTB (Figure 6a). The increase over time in the importance of the NAO and EA in surface temperature is also evident in the GHG fluxes, which explain a large part of the correlation between NAO and the GHG fluxes (Figure 6b). The increase over time in the importance of the NAO and EA in surface temperature is also evident in the GHG fluxes, which explain a large part of the correlation between NAO and the GHG fluxes (Figure 6b). The increase over time in the importance of the NAO and EA in surface temperature is also evident in the GHG fluxes, which explain a large part of the correlation between NAO and the GHG fluxes (Figure 6b).

Figure 5e: Same as Figure 5a, but for the period 1950-1979.

Figure 5f: Same as Figure 5a, but for the period 1980-2020.

Figure 5e (period 1950-1979) shows the strongest correlations between the LSTB and the teleconnections, which explains a large part of the correlation between NAO and the LSTB (Figure 6a). The increase over time in the importance of the NAO and EA in surface temperature is also evident in the GHG fluxes, which explain a large part of the correlation between NAO and the GHG fluxes (Figure 6b). The increase over time in the importance of the NAO and EA in surface temperature is also evident in the GHG fluxes, which explain a large part of the correlation between NAO and the GHG fluxes (Figure 6b). The increase over time in the importance of the NAO and EA in surface temperature is also evident in the GHG fluxes, which explain a large part of the correlation between NAO and the GHG fluxes (Figure 6b).

Figure 5g: Same as Figure 5a, but for the period 1950-1979.

Figure 5h: Same as Figure 5a, but for the period 1980-2020.

Figure 5g (period 1950-1979) shows the strongest correlations between the LSTB and the teleconnections, which explains a large part of the correlation between NAO and the LSTB (Figure 6a). The increase over time in the importance of the NAO and EA in surface temperature is also evident in the GHG fluxes, which explain a large part of the correlation between NAO and the GHG fluxes (Figure 6b). The increase over time in the importance of the NAO and EA in surface temperature is also evident in the GHG fluxes, which explain a large part of the correlation between NAO and the GHG fluxes (Figure 6b). The increase over time in the importance of the NAO and EA in surface temperature is also evident in the GHG fluxes, which explain a large part of the correlation between NAO and the GHG fluxes (Figure 6b).

Figure 5i: Same as Figure 5a, but for the period 1950-1979.

Figure 5j: Same as Figure 5a, but for the period 1980-2020.

Figure 5i (period 1950-1979) shows the strongest correlations between the LSTB and the teleconnections, which explains a large part of the correlation between NAO and the LSTB (Figure 6a). The increase over time in the importance of the NAO and EA in surface temperature is also evident in the GHG fluxes, which explain a large part of the correlation between NAO and the GHG fluxes (Figure 6b). The increase over time in the importance of the NAO and EA in surface temperature is also evident in the GHG fluxes, which explain a large part of the correlation between NAO and the GHG fluxes (Figure 6b). The increase over time in the importance of the NAO and EA in surface temperature is also evident in the GHG fluxes, which explain a large part of the correlation between NAO and the GHG fluxes (Figure 6b).

Figure 5k: Same as Figure 5a, but for the period 1950-1979.

Figure 5l: Same as Figure 5a, but for the period 1980-2020.

Figure 5k (period 1950-1979) shows the strongest correlations between the LSTB and the teleconnections, which explains a large part of the correlation between NAO and the LSTB (Figure 6a). The increase over time in the importance of the NAO and EA in surface temperature is also evident in the GHG fluxes, which explain a large part of the correlation between NAO and the GHG fluxes (Figure 6b). The increase over time in the importance of the NAO and EA in surface temperature is also evident in the GHG fluxes, which explain a large part of the correlation between NAO and the GHG fluxes (Figure 6b). The increase over time in the importance of the NAO and EA in surface temperature is also evident in the GHG fluxes, which explain a large part of the correlation between NAO and the GHG fluxes (Figure 6b).

5 Aerosol effects and weather regimes

Back to Top

As mentioned previously, weather regimes are an appropriate methodology to explore the impacts of aerosols on the NAO and EA. Figure 8 shows the frequency of occurrence of the four weather regimes for winter (DJF) and for the difference between the 1980-2020 and 1950-1979 periods. The methodology described in Section 3.4 is applied to the ALBION simulations in order to quantify the effect of aerosols on the weather regimes.

5.1 Definition of weather regimes

Figure 5a: Summer (JJA) anomalies of the weather regimes for the first (top), NAO- (2nd from top), Blocking (3rd from top), and Atlantic Ridge (bottom) for the period 1979-2020. Only values above statistical 95% confidence level are shown.

Figure 5b: Same as Figure 5a, but for the period 1950-2020.

Winter (DJF) is the most active season for the NAO and EA teleconnections, which explains a large part of the variability in surface temperatures (Figure 5a). The NAO is the strongest in Europe, and its positive phase is associated with warm temperatures across the continent, especially in its northwestern parts, which explain a large part of the correlation between NAO and the LSTB (Figure 6a). The EA is the second most important teleconnection in winter, and its positive phase is also linked to the increase in the LSTB, but its spatial footprint is more in the southern parts of Europe, with the Mediterranean of relatively stable or moderately decreasing trend over Iberia, while the Scandinavian (SCAND) and the East Atlantic/Western Russia (EAWR) patterns have more regional impacts, for the positive phase of SCAND cooling in most of Europe except for the Iberian Peninsula and southern France, and for the positive phase of EAWR cooling in Eastern Europe.

With regards to surface seasonal (one month) means greenhouse gas emissions which are not dominated by the LSTB, the NAO is the most important in winter, but its spatial footprint is much smaller and is a higher resolution than the LSTB (Figure 6b). The EA is the second most important in the positive NAO conditions. However, this pattern is not robust in total NAO due to the opposite sign in its negative phase (Figure 6c).

Figure 5c: Same as Figure 5a, but for the period 1950-1979.

Figure 5d: Same as Figure 5a, but for the period 1980-2020.

Figure 5d (period 1980-2020) shows the strongest correlations between the LSTB and the teleconnections, which explains a large part of the correlation between NAO and the LSTB (Figure 6a). The increase over time in the importance of the NAO and EA in surface temperature is also evident in the GHG fluxes, which explain a large part of the correlation between NAO and the GHG fluxes (Figure 6b). The increase over time in the importance of the NAO and EA in surface temperature is also evident in the GHG fluxes, which explain a large part of the correlation between NAO and the GHG fluxes (Figure 6b). The increase over time in the importance of the NAO and EA in surface temperature is also evident in the GHG fluxes, which explain a large part of the correlation between NAO and the GHG fluxes (Figure 6b).

Figure 5e: Same as Figure 5a, but for the period 1950-1979.

Figure 5f: Same as Figure 5a, but for the period 1980-2020.

Figure 5e (period 1950-1979) shows the strongest correlations between the LSTB and the teleconnections, which explains a large part of the correlation between NAO and the LSTB (Figure 6a). The increase over time in the importance of the NAO and EA in surface temperature is also evident in the GHG fluxes, which explain a large part of the correlation between NAO and the GHG fluxes (Figure 6b). The increase over time in the importance of the NAO and EA in surface temperature is also evident in the GHG fluxes, which explain a large part of the correlation between NAO and the GHG fluxes (Figure 6b). The increase over time in the importance of the NAO and EA in surface temperature is also evident in the GHG fluxes, which explain a large part of the correlation between NAO and the GHG fluxes (Figure 6b).

Figure 5g: Same as Figure 5a, but for the period 1950-1979.

Figure 5h: Same as Figure 5a, but for the period 1980-2020.

Figure 5g (period 1950-1979) shows the strongest correlations between the LSTB and the teleconnections, which explains a large part of the correlation between NAO and the LSTB (Figure 6a). The increase over time in the importance of the NAO and EA in surface temperature is also evident in the GHG fluxes, which explain a large part of the correlation between NAO and the GHG fluxes (Figure 6b). The increase over time in the importance of the NAO and EA in surface temperature is also evident in the GHG fluxes, which explain a large part of the correlation between NAO and the GHG fluxes (Figure 6b). The increase over time in the importance of the NAO and EA in surface temperature is also evident in the GHG fluxes, which explain a large part of the correlation between NAO and the GHG fluxes (Figure 6b).

Figure 5i: Same as Figure 5a, but for the period 1950-1979.

Figure 5j: Same as Figure 5a, but for the period 1980-2020.

Figure 5i (period 1950-1979) shows the strongest correlations between the LSTB and the teleconnections, which explains a large part of the correlation between NAO and the LSTB (Figure 6a). The increase over time in the importance of the NAO and EA in surface temperature is also evident in the GHG fluxes, which explain a large part of the correlation between NAO and the GHG fluxes (Figure 6b). The increase over time in the importance of the NAO and EA in surface temperature is also evident in the GHG fluxes, which explain a large part of the correlation between NAO and the GHG fluxes (Figure 6b). The increase over time in the importance of the NAO and EA in surface temperature is also evident in the GHG fluxes, which explain a large part of the correlation between NAO and the GHG fluxes (Figure 6b).

Figure 5k: Same as Figure 5a, but for the period 1950-1979.

Figure 5l: Same as Figure 5a, but for the period 1980-2020.

Figure 5k (period 1950-1979) shows the strongest correlations between the LSTB and the teleconnections, which explains a large part of the correlation between NAO and the LSTB (Figure 6a). The increase over time in the importance of the NAO and EA in surface temperature is also evident in the GHG fluxes, which explain a large part of the correlation between NAO and the GHG fluxes (Figure 6b). The increase over time in the importance of the NAO and EA in surface temperature is also evident in the GHG fluxes, which explain a large part of the correlation between NAO and the GHG fluxes (Figure 6b). The increase over time in the importance of the NAO and EA in surface temperature is also evident in the GHG fluxes, which explain a large part of the correlation between NAO and the GHG fluxes (Figure 6b).

6 Synthesis

Teleconnection patterns are the leading mechanisms that spread large anomalies around the globe. Teleconnections are the leading mechanisms that spread large anomalies around the globe. Teleconnections are the leading mechanisms that spread large anomalies around the globe. Teleconnections

6 Conclusions

Back to Top

The present study aims to better understand climate-sensitive chlorophyll-a (Chl-a) concentrations in the Mediterranean Sea (MS) and to provide a first assessment of climate-CMIP6-ALBEDO regional climate model driven by the EPA-Estimé reservoirs has this end. Climate-sensitive Chl-a concentrations have been studied in the literature for various marine regions and the different approaches have been discussed in the introduction section

Sayer, A. M., Munchak, L. A., Hsu, N. C., Levy, R. C., Bettenhausen, C., and Jeong, M.: MODIS Collection 6 aerosol products: Comparison between Aqua's e-Deep Blue, Dark Target, and "merged" data sets, and usage recommendations, J. Geophys. Res.-Atmos., 119, 13965–13989, https://doi.org/10.1002/2014JD022453, 2014. a

Schepanski, K., Mallet, M., Heinold, B., and Ulrich, M.: North African dust transport toward the western Mediterranean basin: atmospheric controls on dust source activation and transport pathways during June–July 2013, Atmos. Chem. Phys., 16, 14147–14168, https://doi.org/10.5194/acp-16-14147-2016, 2016. a, b

Séférian, R., Nabat, P., Michou, M., Saint-Martin, D., Voldoire, A., Colin, J., Decharme, B., Delire, C., Berthet, S., Chevallier, M., Sénési, S., Franchisteguy, L., Vial, J., Mallet, M., Joetzjer, E., Geoffroy, O., Guérémy, J.-F., Moine, M.-P., Msadek, R., Ribes, A., Rocher, M., Roehrig, R., Salas-y Mélia, D., Sanchez, E., Terray, L., Valcke, S., Waldman, R., Aumont, O., Bopp, L., Deshayes, J., Éthé, C., and Madec, G.: Evaluation of CNRM Earth-System model, CNRM-ESM 2-1: role of Earth system processes in present-day and future climate, J. Adv. Model. Earth Syst., 11, 4182–4227, https://doi.org/10.1029/2019MS001791, 2019. a

Sevault, F., Somot, S., Alias, A., Dubois, C., Lebeaupin-Brossier, C., Nabat, P., Adloff, F., Déqué, M., and Decharme, B.: A fully coupled Mediterranean regional climate system model: design and evaluation of the ocean component for the 1980–2012 period, Tellus A, 66, 23967, https://doi.org/10.3402/tellusa.v66.23967, 2014. a

Slingo, A.: A GCM Parameterization for the Shortwave Radiative Properties of Water Clouds, J. Atmos. Sci., 46, 1419–1427, https://doi.org/10.1175/1520-0469(1989)046<1419:AGPFTS>2.0.CO;2, 1989. a

Sommeria, G. and Deardorff, J. W.: Subgrid-scale condensation in models of nonprecipitating clouds, J. Atmos. Sci., 34, 344–355, https://doi.org/10.1175/1520-0469(1977)034<0344:SSCIMO>2.0.CO;2, 1977. a

Somot, S., Houpert, L., Sevault, F., Testor, P., Bosse, A., Taupier-Letage, I., Bouin, M.-N., Waldman, R., Cassou, C., Sanchez-Gomez, E., de Madron, X. D., Adloff, F., Nabat, P., and Herrmann, M.: Characterizing, modelling and understanding the climate variability of the deep water formation in the North-Western Mediterranean Sea, Clim. Dynam., 51, 1179–1210, https://doi.org/10.1007/s00382-016-3295-0, 2018. a

Spyrou, C., Kallos, G., Mitsakou, C., Athanasiadis, P., Kalogeri, C., and Iacono, M. J.: Modeling the radiative effects of desert dust on weather and regional climate, Atmos. Chem. Phys., 13, 5489–5504, https://doi.org/10.5194/acp-13-5489-2013, 2013. a

Taylor, K. E., Doutriaux, C., and Peterschmitt, J.-Y.: Climate Model Output Rewriter (CMOR), Version 00, Department of Energy, USA, 2004. a

Thomason, L. W., Ernest, N., Millán, L., Rieger, L., Bourassa, A., Vernier, J.-P., Manney, G., Luo, B., Arfeuille, F., and Peter, T.: A global space-based stratospheric aerosol climatology: 1979–2016, Earth Syst. Sci. Data, 10, 469–492, https://doi.org/10.5194/essd-10-469-2018, 2018. a

Tompkins, A. M., Cardinali, C., Morcrette, J.-J., and Rodwell, M.: Influence of aerosol climatology on forecasts of the African Easterly Jet, Geophys. Res. Lett., 32, L10801, https://doi.org/10.1029/2004GL022189, 2005. a

van Marle, M. J. E., Kloster, S., Magi, B. I., Marlon, J. R., Daniau, A.-L., Field, R. D., Arneth, A., Forrest, M., Hantson, S., Kehrwald, N. M., Knorr, W., Lasslop, G., Li, F., Mangeon, S., Yue, C., Kaiser, J. W., and van der Werf, G. R.: Historic global biomass burning emissions for CMIP6 (BB4CMIP) based on merging satellite observations with proxies and fire models (1750–2015), Geosci. Model Dev., 10, 3329–3357, https://doi.org/10.5194/gmd-10-3329-2017, 2017. a

Vautard, R.: Multiple Weather Regimes over the North Atlantic: Analysis of Precursors and Successors, Mon. Weather Rev., 118, 2056–2081, https://doi.org/10.1175/1520-0493(1990)118<2056:MWROTN>2.0.CO;2, 1990. a, b

Vautard, R., Kadygrov, N., Iles, C., Boberg, F., Buonomo, E., Bülow, K., Coppola, E., Corre, L., van Meijgaard, E., Nogherotto, R., Sandstad, M., c. Schwingshackl, Somot, S., Aalbers, E., Christensen, O. B., Ciarlo, J. M., Demory, M.-E., Giorgi, F., Jacob, D., Jones, R. G., Keuler, K., Kjellström, E., Lenderink, G., Levavasseur, G., Nikulin, G., Sillmann, J., Solidoro, C. Lund Sørland,, S., Steger, C., Teichmann, C., Warrach-Sagi, K., and Wulfmeyer, V.: Evaluation of the large EURO-CORDEX regional climate model ensemble, J. Geophys. Res.-Atmos., in revision, 2020. a

Voldoire, A., Saint-Martin, D., Sénési, S., Decharme, B., Alias, A., Chevallier, M., Colin, J., Guérémy, J.-F., Michou, M., Moine, M.-P., Nabat, P., Roehrig, R., Salas y Mélia, D., Séférian, R., Valcke, S., Beau, I., Belamari, S., Berthet, S., Cassou, C., Cattiaux, J., Deshayes, J., Douville, H., Ethé, C., Franchisteguy, L., Geoffroy, O., Lévy, C., Madec, G., Meurdesoif, Y., Msadek, R., Ribes, A., Sanchez-Gomez, E., Terray, L., and Waldman, R.: Evaluation of CMIP6 DECK experiments with CNRM-CM6-1, J. Adv. Model. Earth Syst., 11, 2177–2213, https://doi.org/10.1029/2019MS001683, 2019. a

Watson, L., Michou, M., Nabat, P., and Saint-Martin, D.: Assessment of CNRM coupled ocean-atmosphere model sensitivity to the representation of aerosols, Clim. Dynam., 51, 2877–2895, https://doi.org/10.1007/s00382-017-4054-6, 2018. a

Winker, D. M., Hunt, B. H., and McGill, M. J.: Initial performance assessment of CALIOP, Geophys. Res. Lett., 34, L19803, https://doi.org/10.1029/2007GL030135, 2007. a

WRMC-BSRN: Baseline Surface Radiation Network: Conditions of data release, Alfred-Wegener-Institute, available at: https://bsrn.awi.de/?id=393, last access: 16 July 2020. a

Zanis, P., Ntogras, C., Zakey, A., Pytharoulis, I., and Karacostas, T.: Regional climate feedback of anthropogenic aerosols over Europe using RegCM3, Clim. Res., 52, 267–278, https://doi.org/10.3354/cr01070, 2012. a

Zubler, E. M., Folini, D., Lohmann, U., Lüthi, D., Muhlbauer, A., Pousse-Nottelmann, S., Schär, C., and Wild, M.: Implementation and evaluation of aerosol and cloud microphysics in a regional climate model, J. Geophys. Res., 116, D02211, https://doi.org/10.1029/2010JD014572, 2011. a

Atmospheric Chemistry and Physics
An interactive open-access journal of the European Geosciences Union

European Geosciences Union
Copernicus Publications
The Innovative Open Access Publisher

All site content, except where otherwise noted, is licensed under the Creative Commons Attribution 4.0 License.

Contact | Imprint | Data protection